A&A 381, 539–559 (2002)
DOI: 10.1051/0004-6361:20011447

Astronomy & Astrophysics

β–radioactive cosmic rays in a diffusion model: Test for a local bubble?

F. Donato[1], D. Maurin[1,2], and R. Taillet[1,2]

[1] Laboratoire de Physique Théorique LAPTH, 74941 Annecy–le–Vieux, France
[2] Université de Savoie, 73011 Chambéry, France

Received 7 August 2001 / Accepted 12 September 2001

Abstract. In a previous analysis, Maurin et al. (2001) have constrained several parameters of the cosmic ray diffusive propagation (the diffusion coefficient normalization K_0 and its spectral index δ, the halo half-thickness L, the Alfvén velocity V_a, and the galactic wind V_c) using stable nuclei. In a second paper (Donato et al. 2002), these parameters were shown to reproduce the observed antiproton spectrum with no further adjustment. In the present paper, we extend the analysis to the β-radioactive nuclei ^{10}Be, ^{26}Al and ^{36}Cl. These species will be shown to be particularly sensitive to the properties of the local interstellar medium (LISM). As studies of the LISM suggest that we live in an underdense bubble of extent $r_{\rm hole} \sim 50$–200 pc, this local feature must be taken into account. We present a modified version of our diffusion model which describes the underdensity as a hole in the galactic disc; we believe some of the formulæ presented here are new. It is found that the presence of the bubble leads to a decrease in the radioactive fluxes which can be approximated by a simple factor $\exp(-r_{\rm hole}/l_{\rm rad})$ where $l_{\rm rad} = \sqrt{K\gamma\tau_0}$ is the typical distance travelled by a radioactive nucleus before it decays. We find that each of the radioactive nuclei independently points towards a bubble of radius $\lesssim$100 pc. If these nuclei are considered simultaneously, only models with a bubble radius $r_{\rm hole} \sim 60$–100 pc are marginally consistent with data. In particular, the standard case $r_{\rm hole} = 0$ pc is disfavored. Our main concern is about the consistency of the currently available data, especially ^{26}Al/^{27}Al.

Key words. ISM: bubbles – galaxy: Solar neighbourhood

1. Introduction

The idea of using long-lived radioactive isotopes to estimate the average age of cosmic rays is not new and the name "radioactive chronometer" is now standard. Indeed, the finite lifetime of these nuclei has a deep impact on their propagation and they are expected to give independent clues about the propagation parameters. To this end, the nucleus ^{10}Be ($t_{1/2} = 1.51$ Myr) was proposed in the fifties, but due to an insufficient knowledge of the processes occurring during propagation, it has long been thought not to be the best candidate after all. Instead, Reames (1970) proposed ^{53}Mn which is EC (electronic capture) unstable ($t_{1/2} = 3.74$ Myr), but it was subsequently shown to be of no great interest, owing to the specific behavior of the EC channel. Later on, Cassé (1973) proposed ^{54}Mn which is a mixed β-EC unstable as a chronometer of the Fe group, the latter being mostly created by collisions of cosmic ray Fe on the interstellar medium. These propositions are very instructive since they demonstrate the early hesitations and progressive comprehension of cosmic ray nuclei propagation. From an observational point of view, the first clues about this propagation time came from the isotope ^{10}Be (Hagen et al. 1977; Webber et al. 1977; Garcia-Munoz et al. 1977). Other isotopically resolved chronometers followed as ^{26}Al (Freier et al. 1980), ^{36}Cl (Wiedenbeck 1985) and ^{54}Mn (Leske 1993). Since then, numerous accurate experiments have been performed (see Sect. 5.2) giving more confident estimates of the surviving fraction of these radioactive clocks.

Most of the conclusions of radioactive studies have been drawn in leaky box models, using the notion of surviving fraction to estimate the age of cosmic rays. The early analyses focused on the surviving fraction and this quantity hinted at the existence of a diffusive halo far beyond the thin galactic disc (see in particular Simpson & Garcia-Munoz 1987 for a discussion). We emphasize that in diffusion models, these notions have no clear physical meaning (see discussion in Sect. 3.1), as stable species and each radioactive species have different ages. The main goal nowadays is

Send offprint requests to: R. Taillet, e-mail: taillet@lapp.in2p3.fr

rather to use a diffusion model that can consistently reproduce all observed radioactive abundances. Our purpose here – following Ptuskin et al. (1997), Ptuskin & Soutoul (1998) – is to demonstrate that one may have to consider local properties of the interstellar medium (ISM) in order to bring this program to a successful conclusion.

The plan of the paper is the following: in a first part we recall the nuclear properties of the radioactive species. In the second part, we focus on the astrophysical aspects of propagation. More specifically, we introduce an inhomogeneous model for the production and propagation of radioactive species. We also discuss the meaning of older models and some false claims that are made in the literature about the predictive power of β radioactive clocks. We then present our analysis and results.

2. Description of radioactive species

From the propagation point of view, one can associate three attributes to each nucleus: (i) a reaction cross section, (ii) a spallation production cross section and (iii) a rest frame half-life. We will not discuss further the first two points as they were discussed at length in Maurin et al. (2001) (hereafter Paper I). Indeed, the cross section code and parameterizations developed in Webber et al. (1990), Webber et al. (1998) (spallation cross section) and Tripathi et al. (1997a, 1997b, 1999) (reaction cross section) are appropriate for both stable and radioactive nuclei.

However, it is not so straightforward to specify decay channels for unstable nuclei. Despite the fact that one can find half-lives easily in nuclear charts (Audi et al. 1997)[1], the information needed from a cosmicist point of view is not always clearly extractable: for example β and EC modes are often combined whereas these two effects act differently during propagation. Thus in the following section, we give a list of nuclei that need to be propagated as unstable. We emphasize that these ingredients were already present in the version of our code used in Paper I, although they were not explicitly discussed.

2.1. Half-lives

Two different disintegration modes must be distinguished: β decay (the nucleus decays spontaneously with a given lifetime $\tau_0 = t_{1/2}/\ln 2$) and EC decay (the nucleus decays after capturing a K-shell electron if one has been attached). In the latter case, the decay rate depends on the electron density and on the typical attachment time. On Earth, many electrons are available so that a nucleus unstable *via* electronic capture behaves as β^+ (at least in terms of the daughter nucleus and half–life). Nevertheless in the ISM, where fewer electrons can be attached, the attachment time must be taken into account in the EC mode. We will come back to this point later on.

Among all the radioactive nuclei, those which have lifetimes of the order of the propagation time may bring interesting information about their propagation. We select and classify them into three categories: β–unstable, EC–unstable and mixed β–EC–unstable. We emphasize that this classification only has a meaning in the context of cosmic ray propagation: were we interested in stellar nucleosynthesis, for example, other tables would be necessary to encode disintegration channels as the characteristic times of evolution involved and the properties of the medium would be drastically different.

Up to now, the most complete description of half-lives adapted to cosmic ray description has been given in Letaw et al. (1984). In this paper, we only consider β unstable nuclei, but as results about EC species will be presented in a separate paper (Donato et al. 2002, in preparation) we find it convenient to describe in this section all unstable species (β and EC). Thus, the following tables are similar to those in Letaw et al. (1984), but we restrict ourselves to $Z \leq 30$ and we take the opportunity to incorporate updated values for some half-lives.

2.1.1. β unstable

In Table 1, we present the three pure β unstable isotopes having proper half-lives in the time range 1 kyr–100 Myr. Nucleus ^{14}C is the shortest-living β unstable isotope included in our cascade. This choice is motivated by the measured propagation time, which runs between 10–20 Myr depending on the propagation model (this time decreases with energy). If a nucleus has a half-life $\lesssim$kyr, we can consider it as a ghost nucleus (see details in Paper I); this means in particular that as soon as it is created, this nucleus immediately (compared to the typical propagation time) disappears into its daughter nucleus, so that its density in cosmic radiation is negligible and it does not need to be propagated. We might object our $\tau_0 > 1$ kyr cut-off, arguing that because of the Lorentz factor $\gamma = E_{\rm tot}/m$, even a short proper lifetime can give a large effective lifetime at sufficiently high energy. Actually, we are concerned with energies $E_{\rm tot} < 100$ GeV/nuc, so that $\gamma < 100$. It follows that proper half-lives $\tau_0 < 1$ kyr correspond to effective half-lives $\tau = \gamma\tau_0 < 0.1$ Myr, which is too short compared to the propagation time for our purpose. Moreover, this cut-off is natural in practice as there are no radioactive half-lives in the interval 0.1–1 kyr. Conversely, if this lifetime

[1] see also `http://sutekh.nd.rl.ac.uk/CoN/` or `http://nucleardata.nuclear.lu.se/nucleardata/`

Table 1. Pure β unstable isotopes (1 kyr $< t_{1/2} <$ 100 Myr).

Z	Nucleus	Daughter	$t_{1/2}^{\rm unit.}$(error)
4	$^{10}_{4}$Be	$^{10}_{5}$B	$1.51^{\rm Myr}$ (0.06)
6	$^{14}_{6}$C	$^{14}_{7}$N	$5.73^{\rm kyr}$ (0.04)
26	$^{60}_{26}$Fe†	$(^{60}_{27}{\rm Co}\overset{\beta^-}{\rightarrow})^{60}_{28}$Ni	$1.5^{\rm Myr}$ (0.3)

† The transition from Fe to Co has a half-life of 1.5 Myr while transition from Co to Ni is immediate from a cosmic ray point of view ($t_{1/2} \sim 5$ yr).

is too high, the corresponding nucleus could be propagated as a stable one. To give an example, ^{40}K – whose β half-life is about $\sim 10^9$ yr – can clearly be considered as stable.

2.1.2. EC unstable

In Table 2, we present the isotopes that are unstable under electronic capture transitions. Unlike for β-decay, these nuclei have to attach an electron to be able to decay. As (i) nuclei are completely stripped of e^- at cosmic ray energies and (ii) the interstellar medium is very poor in e^-, the attachment time may be much longer than the lifetime of the decay. This means that even a nucleus with a very short EC–lifetime may have a long effective lifetime. As a result, there is no need to consider any lower bound on the half-lives. This will be discussed further in Sect. 2.2, and the interested reader can refer to Letaw et al. (1984) or Adams et al. (1985) who show in a leaky box model that the effective half-life of EC nuclei is at least of the order of the attachment rate, which is about $\sim {\rm Myr}^{-1}$.

Table 2. Pure EC unstable isotopes.

Z	unstable (EC)	Daughter	$t_{1/2}^{\rm unit.}$ (error)
4	$^{7}_{4}$Be	$^{7}_{3}$Li	$53.29^{\rm d}$ (0.07)
18	$^{37}_{18}$Ar	$^{37}_{17}$Cl	$35.04^{\rm d}$ (0.04)
20	$^{41}_{20}$Ca	$^{41}_{19}$K	$103^{\rm kyr}$ (4)
22	$^{44}_{22}$Ti	$(^{44}_{21}{\rm Sc}\overset{\beta^+}{\rightarrow})^{44}_{20}$Ca	$49^{\rm yr}$ (3)
23	$^{49}_{23}$V	$^{49}_{22}$Ti	$330^{\rm d}$ (15)
24	$^{48}_{24}$Cr†	$(^{48}_{23}{\rm V}\overset{\beta^+}{\rightarrow})^{48}_{22}$Ti	$21.56^{\rm h}$ (0.03)‡
24	$^{51}_{24}$Cr	$^{51}_{23}$V	$27.702^{\rm d}$ (0.004)
25	$^{53}_{25}$Mn	$^{53}_{24}$Cr	$3.74^{\rm Myr}$ (0.04)
26	$^{55}_{26}$Fe	$^{55}_{25}$Mn	$2.73^{\rm yr}$ (0.03)
27	$^{57}_{27}$Co	$^{57}_{26}$Fe	$271.79^{\rm d}$ (0.09)
28	$^{59}_{28}$Ni§	$^{59}_{27}$Co	$80^{\rm kyr}$ (11)

† This nucleus has an allowed β transition, but contrary to ^{54}Mn and ^{56}Ni (cf. Table 3), it has not been studied recently so that we can set it as a pure EC.

‡ In this two-step reaction, the second transition $^{48}{\rm V}\overset{\beta^+}{\rightarrow}{}^{48}$Ti has a half-life greater than the first one – $15.9735^{\rm d}$ (0.0025). Nevertheless, this second reaction can be taken as immediate because of its β nature. We thus can consider this second element as a ghost (see text). Finally, only the first reaction ($^{48}{\rm Cr}\rightarrow{}^{48}$V) enters the decay rate.

§ This nucleus has a β decay, but with $t_{1/2} > 100$ Gyr. For the same reason as explained in Sect. 2.1.1, it is sufficient to take into account the EC channel.

2.1.3. Mixed β–EC unstable

Finally we turn to the case in which the two decay modes are allowed (hereafter mixed decay), in Table 3. In general, β decay is dominant, but we also need to consider some EC contributions. This is the case for ^{54}Mn which is often

Table 3. Mixed EC-β isotopes.

Z	Nucleus	Daughter (EC)	$t_{1/2}^{\rm unit.}$ (error)	Daughter (β)	$t_{1/2}^{\rm unit.}$ (error)
13	$^{26}_{13}$Al*	$^{26}_{12}$Mg	$4.08^{\rm Myr}$ (0.15)	$^{26}_{12}$Mg	$0.91^{\rm Myr}$ (0.04)
17	$^{36}_{17}$Cl	$^{36}_{16}$S	$15.84^{\rm Myr}$ (0.11)	$^{36}_{18}$Ar	$0.307^{\rm Myr}$ (0.002)
25	$^{54}_{25}$Mn†	$^{54}_{24}$Cr	$312.3^{\rm d}$ (0.4)	$^{54}_{26}$Fe	$0.494^{\rm Myr}$ (0.006)
28	$^{56}_{28}$Ni‡	§($^{56}_{27}$Co$\stackrel{\beta^+}{\rightarrow}$)$^{56}_{26}$Fe	$6.075^{\rm d}$ (0.020)	§($^{56}_{27}$Co$\stackrel{\beta^+}{\rightarrow}$)$^{56}_{26}$Fe	$0.051^{\rm Myr}$ (0.022)

* Martínez-Pinedo & Vogel (1998) (for this nucleus, one can often find in the literature a half-life of 0.74 Myr: it corresponds to the combined β–EC channels, and this is incorrect since these two processes are not equivalent during propagation).
† β half-life taken from Martínez-Pinedo & Vogel (1998). A higher value for this channel is not excluded.
‡ Lund Fisker et al. (1999).
§ $^{56}_{27}$Co decays via EC (80%) and β^+ (20%), but as the half-life is of the order of two months, one can consider that the only effective channel is β–decay so that this nucleus vanishes immediately. Notice that these values are taken from Goldman (1982). More recent references (Audi et al. 1997) or nuclear charts on the web (see footnote 1) are ignored because they give either pure β channel or pure EC channel.

discussed as a possible chronometer for the Fe group, but its EC contribution is rarely treated correctly. Incidentally, Table 3 also shows that the usual two chronometers ^{26}Al and ^{36}Cl have mixed decay channels. But contrary to ^{54}Mn we will see in the next section that the EC channel is completely suppressed, and it is usually neglected.

2.2. Modifications of decay properties during propagation: Effective half-lives

While β decay is independent of the nucleus environment, electronic capture decay depends sharply on the ISM electronic density as well as on the attachment and stripping cross sections. It also follows that the energy dependence of lifetimes is more complex in the EC mode than in the β mode.

This is of great importance for the stability of nuclei, and it gives a flavor of how different the propagation is for these two modes, even for similar half-lives (i.e. $t_{\rm EC} = t_\beta$). In order to clarify these specific behaviors, the pure β–decay will serve as a reference process to which EC processes can be compared. The expression for the density of a β-unstable nucleus can be found in Webber et al. (1992), or formulæ (A8), (A9) and (A10) of Paper I (the disintegration rate appears explicitly in S_i).

As regards the other radioactive species, they actually may be treated like β radioactive species as it is possible to transform their solution into that of pure β with an effective rate instead of the pure EC rate or of the usual combined β–EC rate. An effective lifetime can be introduced, obtained by combining $t_{\rm EC}$, attachment and stripping cross sections (and t_β for mixed decay). A discussion of the validity of such approximations can be found in Letaw et al. (1984), Adams et al. (1985) and references therein. The physical inputs required to describe EC–unstable and β–unstable are

Table 4. Pure β unstable isotopes (1 kyr$< t_{1/2} <$ 100 Myr) from a propagation point of view.

Z	Nucleus	Daughter	$t_{1/2}^{\rm unit.}$(error)
4	$^{10}_{4}$Be	$^{10}_{5}$B	$1.51^{\rm Myr}$ (0.06)
6	$^{14}_{6}$C	$^{14}_{7}$N	$5.73^{\rm kyr}$ (0.04)
13	$^{26}_{13}$Al	$^{26}_{12}$Mg	$0.91^{\rm Myr}$ (0.04)
17	$^{36}_{17}$Cl	$^{36}_{18}$Ar	$0.307^{\rm Myr}$ (0.002)
26	$^{60}_{26}$Fe	$^{60}_{28}$Ni	$1.5^{\rm Myr}$ (0.3)

different and we made the choice here to focus on the latter case. The case of EC–unstable species will be discussed elsewhere (Donato et al. 2002, in preparation). Consequently, the nuclei that one might consider as pure β are given in Table 4.

We have checked that the EC mode can be neglected for ^{27}Al and ^{36}Cl but not for ^{54}Mn and ^{56}Ni. The comparison of our tables to Letaw et al. (1984) shows that the largest difference is for ^{60}Fe half-life which changed from 3×10^5 to 1.5×10^6 yr. For other nuclei, minor corrections in half-lives and their uncertainties have been made.

Finally, we recall that the propagation of nuclei which are radioactively produced requires a specific treatment. Their solution corresponds to formula (A11) of Paper I and as they do not play any role in this study, we will not discuss these daughter nuclei further.

3. Motivation for a local treatment of radioactive cosmic rays propagation

The propagation of cosmic rays is a priori affected by the details of the gas density distribution in the galactic disc. Several models have been proposed to take this into account: for example, Strong & Moskalenko (1998) consider a gas density distribution $n(r, z)$, whereas Osborne & Ptuskin (1987) and Ptuskin & Soutoul (1990) model the ISM as a cloudy medium. As far as the stable species are concerned, one can use an equivalent treatment with an average description of the ISM density. This is what we did in Paper I.

The situation is drastically different for radioactive species. Due to their finite lifetime, those that reach the solar system must have been created locally, i.e. in a region which is at most a few hundred parsecs away (see below). As a consequence, the local interstellar matter (LISM) has to be carefully described.

Actually, there are reasons to believe that this LISM is highly inhomogeneous, which motivates a more elaborate model for radioactive species. This model will be described in the next section, after we have discussed the locality of radioactive production and the inhomogeneity of the LISM.

3.1. Locality from diffusion equation

It is often claimed that the size of the diffusion halo can be estimated from radioactive cosmic ray species. This is true in the framework of a leaky box propagation model, but not for diffusion models (see below). Indeed, the leaky box models have been so widely used in the past that some of their conclusions have become popular wisdom and are sometimes used out of their proper context. Actually, as was explicitly shown in the early seventies (Prishchep & Ptuskin 1975; Ginzburg et al. 1980), leaky box models are almost never equivalent to diffusion models, so that one should be very careful before directly applying leaky box inspired results to another class of models, e.g. diffusion models.

3.1.1. The old leaky box paradigm, and what we should forget to go further...

The so-called leaky box modelling of cosmic ray propagation assumes that the particles freely move in a homogeneous finite-sized box. When a particle reaches a boundary of the box, there is a finite probability that it escapes the system. As a result, forgetting about anything but propagation, the density is given by, in this model,

$$\frac{\partial N(E,t)}{\partial t} - \frac{N(E,t)}{\tau_{\rm esc}(E)} = 0$$

where $\tau_{\rm esc}(E)$ is the typical time a particle of energy E spends in the box. It is possible to account for the measured abundance of all the stable cosmic ray nuclei abundances with a suitable $\tau_{\rm esc}(E)$, adjusted for all nuclei. However, the physical picture provided by this model is wrong. Cosmic rays do not freely stream in a homogeneous box, but they are scattered by the inhomogeneities of the galactic magnetic field. This results in a diffusive propagation. This difference is of no importance when one is concerned only with the local abundance of stable nuclei, and it can be shown that in this case, there is an equivalence between these two approaches (see discussion in Paper I and references therein). But as soon as one tries to change the mathematically correct local description of stable nuclei provided by the leaky box into a physical picture and tries to extend it either to radioactive species or to another location, trouble begins.

First, it is obvious that from the start, the leaky box model is unable to describe the spatial distribution of cosmic rays. We will not discuss this point further.

Second, it is also clear that this model is bound to fail for radioactive cosmic ray nuclei. The species we consider have a proper lifetime of the order of $\tau \sim 1$ Myr, so that at the speed of light they can travel more than $\sim$300 kpc before they decay. As the radius of the galaxy is $\sim$20 kpc, these nuclei should have enough time to propagate in the whole available volume and their distribution is sensitive to the global geometry and localization of the sources. This is at variance with the diffusion model in which the average distance travelled by a nucleus during a time τ is given by $\sqrt{K(E)\tau}$, which is of the order of a few hundred parsecs at low energy. This means that in this case, the distribution of these species only depends on the *local* characteristics of the diffusive medium and of the sources.

It is sometimes claimed that a radioactive species gives the size L of the diffusive halo: the bigger the halo, the smaller the quantity of nuclei that survive from the sources to the Earth. This is easily understood in the framework of the leaky box, but it is physically wrong for diffusion models. A more quantitative version of the intuitive argument given above can be found in Prishchep & Ptuskin (1975). They showed that diffusion models are equivalent to leaky

box models only when the relationship $\tau_0 \gg L^2/K$ is satisfied. In the most favorable of the cases we consider here, this corresponds to $\tau_0 \gg 100$ Myr, which is wrong for the nuclei we are interested in.

Thus, one should be careful not to use leaky box induced conclusions out of this specific context. They may be very intuitive but wrong when applied to a diffusion model. For example, the next section shows that the radioactive-to-parent ratio is not sensitive to the size of the halo in a diffusion model.

3.1.2. Does a radioactive really tell something about the halo size L?

In the diffusion model, a radioactive nucleus with a proper lifetime τ_0 has most probably travelled a distance $l_{\rm rad} = \sqrt{K(E)\gamma\tau_0}$ between its creation in the disc and its detection on Earth. At low energy, this distance is much smaller than the size of the diffusive volume, and this nucleus is not very sensitive to the boundaries of this volume. This can be seen in the expression giving the ratio radioactive/parent nucleus. In the case when there is only one parent nucleus and if energetic gains and losses are discarded, the density is given by (see Eq. (A8) of Paper I)

$$N^{\rm uns}(z=0,r) = \sum_{i=0}^{\infty} \frac{2h\Gamma^{\rm prod} N_i^{\rm parent}(z=0)}{A_i} J_0\left(\zeta_i \frac{r}{R}\right) \tag{1}$$

with

$$A_i \equiv 2h\Gamma^{\rm inel} + V_{\rm c} + KS_i \coth(S_i L/2) \tag{2}$$

and

$$S_i = \left(\frac{V_{\rm c}^2}{K^2} + \frac{4\zeta_i^2}{R^2} + \frac{4\Gamma^\beta}{K}\right)^{1/2}. \tag{3}$$

When the lifetime is so short that $\Gamma^\beta L/K \approx L/l_{\rm rad} \gg 1$, we have $\coth(S_i L/2) \approx 1$. It can be easily seen that in these conditions, the ratio $N^{\rm uns}(z=0,r)/N^{\rm par}(z=0,r)$ becomes independent of the halo size L. Figure 1 displays this ratio for various L when formula (1) is used. The diffusion coefficient $K(E)$ and $l_{\rm rad}$ are increasing functions of energy, so that when $l_{\rm rad}$ becomes of the order of the typical size of the halo (L or R), diffusive propagation is affected by the shape and size of the halo.

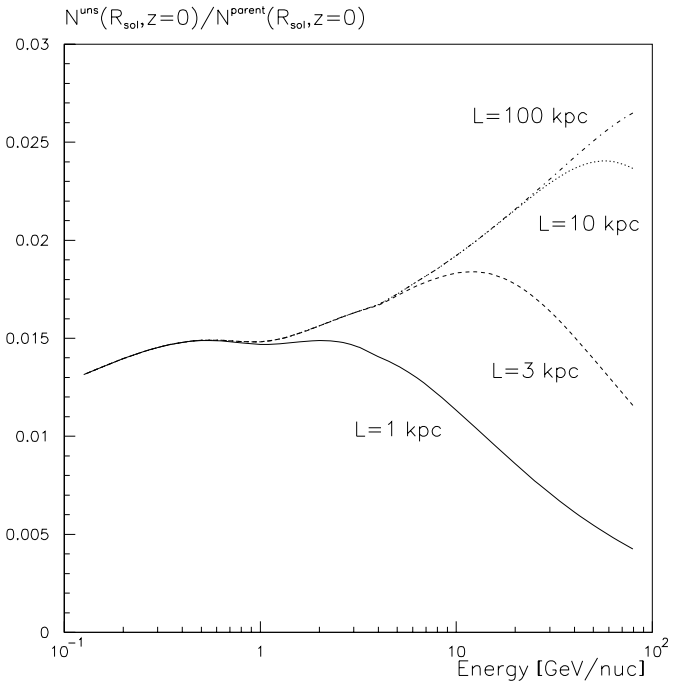

Fig. 1. Unstable/parent ratio (^{26}Al/^{28}Si) for different values of L in kpc, all other parameters being fixed.

We have presented here a model in which only one parent was considered. Actually, there are several parents and the above conclusion is not exact but remains approximate if they are considered, so that at low energy, the ratio

$N^{\rm uns}/\sum_{\rm par} N^{\rm par}$ is the same whatever the size of the halo. All current data on radioactive nuclei are at low energy, so that we do not expect such a ratio to give direct constraints on L.

Nevertheless, the ratio of isotopes having the same parents, like ^{10}Be/^{9}Be, are usually considered. As the quantity $^{9}\mathrm{Be}/\sum_{\rm par} N^{\rm par}$ *does* depend on the halo size the ratio ^{10}Be/^{9}Be eventually also does.

3.2. Local sub-density: We all leave in a local bubble

Interest in the study of our local environment has grown in the last thirty years (see for example Cox & Reynolds 1987 for a review). As emphasized in McKee (1998), the very recent all sky survey by ROSAT became an invaluable resource for all astronomers in general, and for the LISM study in particular. In this section, we present evidence indicating why it is probably necessary to have a specific description for the local ISM (in a region of about ∼100 pc around the solar neighborhood). We then develop a model to incorporate the effect of these local properties of the ISM on radioactive species within our diffusion model.

3.2.1. Main properties of the LISM

First, it has to be noticed that far more progress has been made in mapping three dimensional distribution of galaxies many megaparsecs away than the distribution of local interstellar clouds within a hundred parsecs (McKee 1998). We can nevertheless summarize a few points about the local composition. First, the LISM is defined as a region of extremely hot gas (∼10^5–10^6 K) and low density ($n \lesssim 0.005$ cm^{-3}) within a bubble of radius between $\lesssim$65–250 pc surrounded by a dense neutral gas boundary ("hydrogen wall") (Sfeir et al. 1999; Linsky et al. 2000). A smaller scale description of this bubble shows that the Sun is located in a local fluff with $N_{\rm HI} \sim 0.1$ cm^{-3}, $T \sim 10^4$ K and a typical extension of ∼50 pc. It is of great importance for further modelling to realize that the local bubble is highly asymmetric (Cox & Reynolds 1987; Welsh et al. 1994; Fruscione et al. 1994), and that several cloudlets are present in the bubble (for a schematic representation, see for example Fig. 1 of Breitschwerdt et al. 2000). Various models have attempted to explain the formation of this local bubble (Smith & Cox 2001; Breitschwerdt et al. 2000; see also Cox 1997 for a brief review), but this subject is far beyond our concern.

Finally, a model can be built, considering that the Sun is surrounded by a first shell of radius ∼50 pc and density ∼0.1 cm^{-3}, and a second shell of radius ∼200 pc with an almost null density. Beyond this second shell, we recover the usual average density 1 cm^{-3} (or zero density if the radius of the second shell extends beyond the disc). In the rest of this paper, we use a coarser description, in which the underdensity is modelled with one cylindrical hole of radius $r_{\rm hole}$ to be determined and with a null density. It will be called "the hole" throughout this paper.

3.2.2. Consequences for the radioactive production

The propagation of cosmic rays is influenced by (i) the local magnetic properties and (ii) the local matter content of the disc. In this section, we investigate the effect of this hole on these properties.

First, we assume that diffusion itself, as described by the coefficient $K(E)$, is not affected by the presence of the hole, i.e. diffusion is homogeneous. Homogeneity seems to be confirmed by radio and γ-ray observations, which can test in situ the spectrum and density of cosmic rays (McKee 1998; Morfill & Freyberg 1998).

The presence of the hole has another consequence. Because the density is lower, there are less spallations in the bubble, so that the secondary nuclei abundances (including radioactive ones) are probably perturbed. As a matter of fact, a realistic description of the matter content of the disc should take into account a spatial distribution (exponential or more complex) as used for example in Strong & Moskalenko (1998). However, the only relevant quantity for stable nuclei is the average grammage of matter they cross. As these nuclei propagate in a region which is much bigger than the hole, this average grammage is only slightly changed by the presence of the hole. This can be seen in Fig. 5, where the change in the radial distribution of a stable species due to the hole is represented. In the following, the local density of stable nuclei will be computed with a full matter disc of density 1 cm^{-3}.

The situation is different for radioactive species, as the typical distance they travel from their creation in the disc to their detection on Earth is limited by their finite lifetime τ. This distance can be estimated as $l_{\rm rad} \sim \sqrt{K(E)\gamma\tau_0}$. For the nuclei we consider here, and for energies of a few hundred MeV/nuc, $l_{\rm rad}$ is of the same order of magnitude as the size of the hole, so that their propagation is expected to be more strongly perturbed. To be specific, the fact that spallations do not occur within the hole has three distinct physical effects. First, it leads to a decrease in the spallation source term of the radioactive species. Second, it also leads to a local decrease of destructive spallations. Third, as there is less interstellar matter to interact with, the energy losses are also lowered.

4. Modelling the local propagation

We now want to take these remarks and incorporate the three physical effects discussed above in our diffusion model. We start with a very simple model, in which the influence of the hole can be easily understood. We then adapt the model discussed at length in Paper I and Donato et al. (2002) (hereafter Paper II). In the following subsections, we present the demonstration of the corresponding new formulæ. This section is a bit technical and the confident reader can skip the demonstrations and go directly to Sect. 4.6.

4.1. A first simple approach

We begin with a very simple model, in which the galactic disc is an infinitely thin disc extending to infinity, embedded in an infinite diffusive volume. These assumptions are not unreasonable as propagation of radioactive species is a local phenomenon and is not expected to be much affected by boundaries. We also ignore destructive spallations, galactic wind and energy losses. At the origin of the galactic plane stands a hole of radius $r_{\rm hole}$.

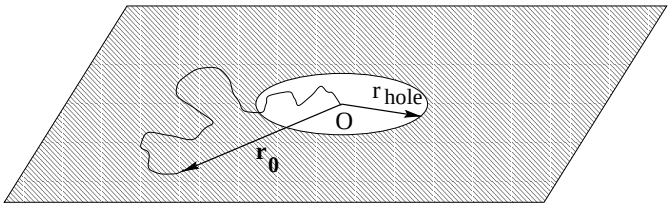

Fig. 2. Schematic representation of the first model. The disc is infinite in all directions and has zero thickness.

Consider first the nuclei coming from spallations at time t_0 and at a source point $\boldsymbol{r}_0$. They act as an instantaneous source term $f_0\delta(\boldsymbol{r}-\boldsymbol{r}_0)\delta(t-t_0)$. The number that would reach the center at time $t>t_0$, with no decay, satisfies

$$\frac{\partial f}{\partial t} = K\Delta f = \frac{K}{r^2}\frac{\partial}{\partial r}\left(r^2\frac{\partial f}{\partial r}\right) = f_0\delta(\boldsymbol{r}-\boldsymbol{r}_0)\delta(t-t_0).$$

A solution of this equation is given by

$$f(\boldsymbol{r}-\boldsymbol{r}_0, t-t_0) = \frac{f_0}{(4\pi K(t-t_0))^{3/2}}\exp\left\{-\frac{\|\boldsymbol{r}-\boldsymbol{r}_0\|^2}{4K(t-t_0)}\right\}.$$

For radioactive species with a lifetime $\tau=\gamma\tau_0$ (where τ_0 is the rest frame lifetime), decay must be taken into account and we have instead, at $\boldsymbol{r}=\boldsymbol{0}$,

$$f(\boldsymbol{0},t) \propto \frac{1}{(t-t_0)^{3/2}}\exp\left\{-\frac{r_0^2}{4K(t-t_0)}\right\}\times\exp\left\{-\frac{t-t_0}{\tau}\right\}. \tag{4}$$

This function is actually the propagator of this diffusion problem. In the permanent regime, the total quantity of these nuclei at the center of the hole is obtained by summing the solutions for a distribution of point sources acting at all instants from $t_0=-\infty$ to t (now). It leads to an integration over space and time

$$N \propto \int_0^\infty 2\pi r_0\, n(r_0)\,\mathrm{d}r_0 \int_{-\infty}^{t}\frac{\mathrm{d}t_0}{(t-t_0)^{3/2}}\exp\left\{-\frac{r_0^2}{4K(t-t_0)}\right\}\times\exp\left\{-\frac{t-t_0}{\tau}\right\}$$

in our case, $n(r_0)=0$ for $r_0<r_{\rm hole}$ and $n(r_0)=n_0$ for $r_0>r_{\rm hole}$, so that

$$N \propto n_0\int_{r_{\rm hole}}^\infty 2\pi r_0\,\mathrm{d}r_0\int_{-\infty}^{t}\mathrm{d}t_0\,\frac{1}{(t-t_0)^{3/2}}\exp\left\{-\frac{r_0^2}{4K(t-t_0)}\right\}\times\exp\left\{-\frac{t-t_0}{\tau}\right\}.$$

Integration over r_0 is easily performed

$$N \propto \int_{-\infty}^{t}\frac{\mathrm{d}t_0}{\sqrt{(t-t_0)}}\exp\left\{-\frac{r_{\rm hole}^2}{4K(t-t_0)}\right\}\times\exp\left\{-\frac{t-t_0}{\tau}\right\}.$$

Introducing $x=\sqrt{(t-t_0)/\tau}$,

$$N \propto \int_0^\infty \mathrm{d}x\,\exp\left\{-\frac{r_{\rm hole}^2}{4K\tau}\,x^{-2}-x^2\right\}.$$

This integral is given by

$$\int_0^\infty \mathrm{d}x\, \exp\left\{-\frac{\alpha}{x^2}-x^2\right\} = \frac{\sqrt{\pi}}{2}\mathrm{e}^{-2\sqrt{\alpha}} \tag{5}$$

so that finally

$N \propto \mathrm{e}^{-r_{\rm hole}/\sqrt{K\tau}}$.

The central density due to the full disc would be given by $r_{\rm hole}=0$, so that, introducing $l_{\rm rad} \equiv \sqrt{K\gamma\tau_0}$,

$$N_{r_{\rm hole}}(r=0) = N_{(r_{\rm hole}=0)}(r=0) \times \mathrm{e}^{-r_{\rm hole}/l_{\rm rad}}. \tag{6}$$

We emphasize that in the problem treated here, the time-dependent resolution by means of propagators that we used in this section is equivalent to solving the corresponding stationary equation ($\partial f/\partial t = 0$). This latter approach is more convenient for implementing the physical effects we have neglected here. It will be used in the next sections and as expected, the same behavior will be recovered.

4.2. Analytical solutions without energy losses and reacceleration

We now turn to a more realistic model, namely a cylindrical diffusion box of radius R and half-height L, and a matter disc of half-height h, considered as infinitely thin. The local subdensity has to be represented by a circular hole of radius $r_{\rm hole}$ located at the position of the Sun. Compared to the previous approach, it has the advantage of correctly taking into account the presence of boundaries. It also takes into account destructive spallations and galactic wind. It is actually the model used in Papers I and II, with an additional hole of radius $r_{\rm hole}$.

To make the problem tractable analytically, we make some simplifying hypotheses. First, to preserve the cylindrical symmetry, we consider that the Sun (and the hole) is located at the center of the disc. Second, we suppose that the density of the parent species is uniform all over the galactic disc, i.e. it does not depend on the spatial coordinate r. The validity of these assumptions relies on the fact that the propagation of radioactive species is a local process. We will discuss further these points in Sect. 4.4.

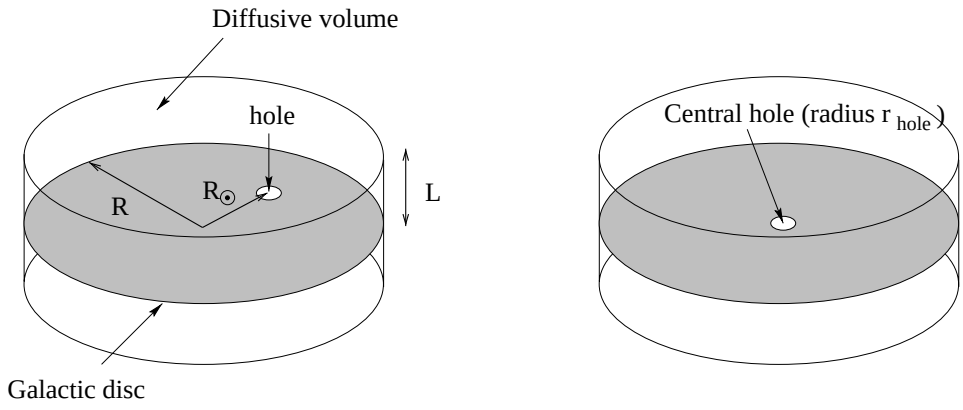

Fig. 3. Schematic representation of the model. Left picture is the actual geometry of the problem, with a hole of radius $r_{\rm hole}$ in the disc, at the position of the Sun. The right picture represents the simplified geometry (cylindrical symmetry is preserved) which is shown to give the same results.

We want to solve the diffusion equation for a radioactive secondary (no primary sources)

$$K\Delta N^{\rm uns}(r,z) - V_{\rm c}\frac{\partial N^{\rm uns}(r,z)}{\partial z} - \Gamma^{\beta}N^{\rm uns}(r,z) + 2h\delta(z)\left[\Gamma^{\rm prod}(r)N^{\rm par}(r,0) - \Gamma^{\rm inel}(r)N^{\rm uns}(r,0)\right] = 0. \tag{7}$$

To keep notations simple, we consider only one parent nucleus. It would be straightforward to generalize to several parents. Here, $N^{\rm uns}$ denotes the unstable nucleus, $N^{\rm par}$ the parent nucleus and $\Gamma^{\rm prod}$, $\Gamma^{\rm inel}$ and Γ^{β} denote respectively the production rate (by spallation) of the parent $N^{\rm par}$ into the radioactive nucleus $N^{\rm uns}$, the destruction rate of $N^{\rm uns}$ by inelastic scattering and its β–disintegration rate. This equation differs from the no–hole case (Eq. (A1) of Paper I) because the terms $\Gamma^{\rm prod}(r) = n_{\rm LISM}(r)v\sigma^{\rm prod}$ and $\Gamma^{\rm inel}(r) = n_{\rm LISM}(r)v\sigma^{\rm inel}$ now depend explicitly on r via the local interstellar density which reads

$$n_{\rm LISM}(r) = \Theta(r - r_{\rm hole})n_{\rm ISM} \tag{8}$$

where Θ is the Heavyside distribution. Thus, we can rewrite Eq. (7) in the form

$$K\Delta N^{\rm uns}(r,z) - V_{\rm c}\frac{\partial N^{\rm uns}(r,z)}{\partial z} - \Gamma^{\beta} N^{\rm uns}(r,z) + 2h\delta(z)\left[\Gamma^{\rm prod}\Theta(r-r_{\rm hole})N^{\rm par}(r,0) - \Gamma^{\rm inel}\Theta(r-r_{\rm hole})N^{\rm uns}(r,0)\right] = 0. \quad (9)$$

As for the no-hole model (see Paper I), a solution is found by expanding the density over the Bessel functions $J_0(\zeta_i r/R)$ where the ζ_i are the zeros of J_0. The unknown quantities $N^{\rm uns}(r,z)$ are expanded as

$$N^{\rm uns}(r,z) = \sum_i N_i^{\rm uns}(z) J_0\left(\zeta_i \frac{r}{R}\right). \quad (10)$$

The known quantities are also expanded as

$$\Upsilon(r,z) = \sum_i \Upsilon_i(z) J_0\left(\zeta_i \frac{r}{R}\right) \quad \text{with} \quad \Upsilon_i(z) = \frac{2}{J_1^2(\zeta_i)} \int_0^1 \rho \Upsilon(\rho,z) J_0(\zeta_i \rho)\, {\rm d}\rho$$

where $\rho = r/R$.

We now have to differentiate the case of source spallation from that of destruction. For the first one, we can assume that the density of the parent depends very smoothly on the coordinate r so that we can safely take $N^{\rm par}(r,0) = N^{\rm par}(R_\odot,0)$; this approximation will be checked in Sect. 4.4. We must compute the Bessel transform of the Heavyside function

$$\Theta_i = \frac{2}{J_1(\zeta_i)^2} \int_0^1 \rho\, \Theta\left(\rho - \frac{r_{\rm hole}}{R}\right) J_0(\zeta_i \rho) {\rm d}\rho.$$

With the notation $x = \zeta_i \rho$ and using the fact that a primitive of $xJ_0(x)$ is $xJ_1(x)$, it can be shown that

$$\Theta_i = \frac{2}{\zeta_i J_1(\zeta_i)^2} \times \left[J_1(\zeta_i) - \frac{r_{\rm hole}}{R} J_1\left(\zeta_i \frac{r_{\rm hole}}{R}\right)\right]. \quad (11)$$

For the destructive spallation term, we have to Bessel develop the function $\Theta(r-r_{\rm hole})N^{\rm uns}(r,0)$. At variance with the precedent case, the distribution $N^{\rm uns}(r,0)$ is expected to vary significantly across the hole so that the previous approximation cannot be made. We thus have

$$\Theta(r-r_{\rm hole})N^{\rm uns}(r,0) = \sum_{i=1}^{\infty} \Omega_i^{\rm uns} J_0\left(\zeta_i \frac{r}{R}\right)$$

where

$$\Omega_i^{\rm uns} \equiv \frac{2}{J_1^2(\zeta_i)} \int_0^1 \rho\, N^{\rm uns}(\rho,0) \Theta\left(\rho - \frac{r_{\rm hole}}{R}\right) J_0(\zeta_i \rho)\, {\rm d}\rho.$$

Inserting the Bessel development of $N^{\rm uns}(r, z=0)$ into this relation (see Eq. (10)), we find

$$\Omega_i^{\rm uns} = \frac{2}{J_1^2(\zeta_i)} \sum_{j=1}^{\infty} N_j^{\rm uns}(z=0) \int_{r_{\rm hole}/R}^1 \rho\, J_0(\zeta_j \rho) J_0(\zeta_i \rho)\, {\rm d}\rho.$$

Using the property

$$\int \rho\, J_0(\zeta_j \rho) J_0(\zeta_i \rho)\, {\rm d}\rho = \begin{cases} \dfrac{1}{\zeta_j^2 - \zeta_i^2}\left[-\zeta_i \rho J_0(\zeta_j \rho) J_1(\zeta_i \rho) + \zeta_j \rho J_1(\zeta_j \rho) J_0(\zeta_i \rho)\right] & \text{for } i \neq j \\ \displaystyle\int \rho\, J_0^2(\zeta_i \rho)\, {\rm d}\rho = \frac{1}{2}\rho^2 \left[J_0^2(\zeta_i \rho) + J_1^2(\zeta_i \rho)\right] & \text{else} \end{cases}$$

it follows that

$$\begin{aligned} \Omega_i^{\rm uns} \;=\; & N_i^{\rm uns}(0) - \frac{r_{\rm hole}^2}{R^2 J_1^2(\zeta_i)} N_i^{\rm uns}(0) \left[J_0^2\left(\frac{\zeta_i r_{\rm hole}}{R}\right) + J_1^2\left(\frac{\zeta_i r_{\rm hole}}{R}\right)\right] \\ & + \frac{2 r_{\rm hole}}{R J_1^2(\zeta_i)} \sum_{j \neq i} \frac{N_j^{\rm uns}(0)}{\zeta_j^2 - \zeta_i^2} \left[\zeta_i J_0\left(\frac{\zeta_j r_{\rm hole}}{R}\right) J_1\left(\frac{\zeta_i r_{\rm hole}}{R}\right) - \zeta_j J_1\left(\frac{\zeta_j r_{\rm hole}}{R}\right) J_0\left(\frac{\zeta_i r_{\rm hole}}{R}\right)\right]. \end{aligned} \quad (12)$$

Finally, putting everything altogether, the Bessel transform of Eq. (9) reads

$$\left[\frac{\partial^2}{\partial z^2} - \frac{V_{\rm c}}{K}\frac{\partial}{\partial z} - \left(\frac{\zeta_i^2}{R^2} + \frac{\Gamma^{\beta}}{K}\right)\right] N_i^{\rm uns}(0) + \frac{2h}{K}\delta(z)\left[\Theta_i \times \Gamma^{\rm prod} N^{\rm par}(R_\odot,0) - \Omega_i^{\rm uns} \times \Gamma^{\rm inel}\right] = 0 \quad (13)$$

where Θ_i and $\Omega_i^{\rm uns}$ are given by Eqs. (11) and (12). This equation is now very similar to Eq. (A6) of Paper I, and resolution proceeds as exposed therein. The solution in the halo is

$$N_i^{\rm uns}(z) \propto {\rm e}^{V_{\rm c}z/2K} \times \sinh\left\{\frac{S_i(L-z)}{2}\right\}$$

where S_i and A_i were defined in Sect. 3.1.2. The solution in the disc is obtained by integrating Eq. (7) across the disc,

$$2N_i^{\rm uns\prime}(0) - 2N_i^{\rm uns}(0)\frac{V_{\rm c}}{K} - \frac{2h\Gamma^{\rm inel}}{K}\Omega_i^{\rm uns} + \frac{2h\Gamma^{\rm prod}}{K}\Theta_i N^{\rm par}(R_\odot,0) = 0$$

which gives

$$N_i^{\rm uns}(0) = \Theta_i \times \frac{2h\Gamma^{\rm prod}N^{\rm par}(R_\odot,0)}{A_i} - \frac{2h\Gamma^{\rm inel}}{A_i}\left[\Omega_i^{\rm uns} - N_i^{\rm uns}\right]. \tag{14}$$

The first term is very similar to the secondary source contribution of a no-hole model, but with an additional Θ_i factor taking correctly into account the effect of the hole on production spallations. The second term takes into account the effect of the hole on destructive spallations. It is expressed as

$$\begin{aligned}\Omega_i^{\rm uns} - N_i^{\rm uns} = &- \frac{r_{\rm hole}^2}{R^2 J_1^2(\zeta_i)} N_i^{\rm uns}(0)\left[J_0^2\left(\frac{\zeta_i r_{\rm hole}}{R}\right) + J_1^2\left(\frac{\zeta_i r_{\rm hole}}{R}\right)\right] \\ &+ \frac{2r_{\rm hole}}{RJ_1^2(\zeta_i)}\sum_{j\neq i}\frac{N_j^{\rm uns}(0)}{\zeta_j^2-\zeta_i^2}\left[\zeta_i J_0\left(\frac{\zeta_j r_{\rm hole}}{R}\right)J_1\left(\frac{\zeta_i r_{\rm hole}}{R}\right) - \zeta_j J_1\left(\frac{\zeta_j r_{\rm hole}}{R}\right)J_0\left(\frac{\zeta_i r_{\rm hole}}{R}\right)\right].\end{aligned} \tag{15}$$

As this term depends on $N_j^{\rm uns}(0)$, (14) is a coupled set of equations and may be tricky to solve in practice.

Actually, as the effect of spallations is expected to be small, we use a perturbative method. We first compute the solution of Eq. (14) without the last term of Eq. (15),

$$N_i^{\rm uns,(0)}(0) = \Theta_i \times \frac{2h\Gamma^{\rm prod}N^{\rm par}(R_\odot,0)}{A_i'}$$

with

$$A_i' = A_i + 2h\Gamma^{\rm inel}\frac{r_{\rm hole}^2}{R^2J_1^2(\zeta_i)}\left[J_0^2\left(\frac{\zeta_i r_{\rm hole}}{R}\right) + J_1^2\left(\frac{\zeta_i r_{\rm hole}}{R}\right)\right].$$

The term we have neglected can now be taken into account by substituting the $N_j^{\rm uns}(0)$ in Eq. (15) by these zero-order solutions $N_j^{\rm uns,(0)}$.

$$N_i^{\rm uns,(1)}(0) = N_i^{\rm uns,(0)}(0) + \frac{4h\Gamma^{\rm inel}}{J_1^2(\zeta_i)A_i}\frac{r_{\rm hole}}{R}\times\sum_{j\neq i}\frac{N_j^{\rm uns,(0)}(0)}{\zeta_j^2-\zeta_i^2}\left[\zeta_i J_0\left(\frac{\zeta_j r_{\rm hole}}{R}\right)J_1\left(\frac{\zeta_i r_{\rm hole}}{R}\right) - \zeta_j J_1\left(\frac{\zeta_j r_{\rm hole}}{R}\right)J_0\left(\frac{\zeta_i r_{\rm hole}}{R}\right)\right].$$

The new quantities $N_i^{\rm uns,(1)}(0)$ can then be used instead of $N_i^{\rm uns,(0)}(0)$ to estimate the correction at the next order. This procedure is repeated until convergence is reached. In practice, convergence is very quick and we only need to iterate twice.

4.3. Behavior of the solution as a function of the hole radius

A numerical study of this solution (see Fig. 4) shows that the dependence in $r_{\rm hole}$ can be expressed as, with good accuracy,

$$N_i(0) \approx \exp\left(-\frac{r_{\rm hole}}{l_{\rm rad}}\right) \quad \text{with} \quad l_{\rm rad} = \sqrt{K(E)\gamma\tau_0}. \tag{16}$$

The physical meaning of this dependence is better seen with the first approach (Sect. 4.1). The relevant quantities to compare are the size of the hole and $l_{\rm rad}$, which represents the typical distance travelled by a radioactive nucleus before it decays. This distance increases with energy, because of time dilation and because high energy nuclei diffuse more efficiently (K grows with energy). For a diffusion coefficient of the form $K = K_0\beta\mathcal{R}^\delta$, $l_{\rm rad}$ can be expressed as

$$l_{\rm rad} = \sqrt{K\gamma\tau_0} = \sqrt{K_0\tau_0}\,\frac{A^{(\delta-1)/4}}{Z^{\delta/2}}\left(E_{k,\rm nuc}^2 + 2m_{\rm p}E_{k,\rm nuc}\right)^{(\delta+1)/4}. \tag{17}$$

Typical values are given at several energies and for several radioactive nuclei for $K_0 = 0.033$ kpc^2 Myr^{-1} and $\delta = 0.6$ (a good model taken from Paper I) in Table 5.

Table 5. Values of $l_{\rm rad}$ for several radioactive nuclei and energies.

	τ_0 (Myr)	$E_k = 100$ MeV/n	1 GeV/nuc	10 GeV/nuc
^{10}Be	2.17	0.075 kpc	0.22 kpc	0.95 kpc
^{26}Al	1.31	0.037 kpc	0.11 kpc	0.47 kpc
^{36}Cl	0.443	0.019 kpc	0.056 kpc	0.25 kpc

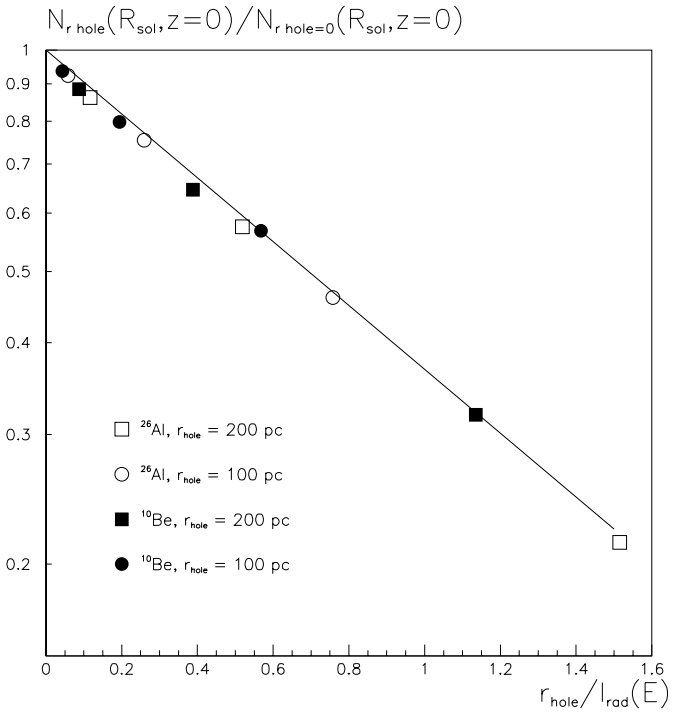

Fig. 4. The radioactive flux is computed for ^{26}Al and ^{10}Be, for several energies (corresponding to several values of $l_{\rm rad}(E)$) and for several hole radii $r_{\rm hole}$. This plot displays each flux divided by the flux obtained in the homogeneous case ($r_{\rm hole} = 0$), as a function of $r_{\rm hole}/l_{\rm rad}$. The solid line represents the function $\exp(-r_{\rm hole}/l_{\rm rad})$.

4.4. Discussion of the validity of the hypotheses

The most a priori questionable assumption is that we located the hole at the center of the galactic disc, though we know that the Sun is at a galactocentric distance of about $R = 8$ kpc. Figure 5 displays the radial distribution of a radioactive species in the disc for several energies. We see this distribution is only perturbed locally by the presence of the hole: at a distance of a few $l_{\rm rad}$, the flux is no longer affected by the hole. Conversely, the flux at the center of the hole is not affected by the boundaries of the diffusive box if they are farther than a few $l_{\rm rad}$. We could even consider that the galactic disc is an infinite plane. This means that the same distribution – and the same reduction factor $\exp(-r_{\rm hole}/l_{\rm rad})$ – is obtained whatever the position of the hole, as long as it is far enough from the edges of the box (compared to $l_{\rm rad}$), which is the case for us. The density of parent nuclei must obviously be estimated at the position of the Sun (and not at the center of the galaxy!).

We also assumed that the parent has a homogeneous distribution all over the disc, which is known to be wrong: the parent flux is greater around the position of the sources ($r \sim 4$ kpc, see for example Paper I, Sect. 3.5.1 and references therein) and decreases regularly to zero at the edge of the disc ($R = 20$ kpc). However, as the radioactive propagation is a local phenomenon, at the scale of $l_{\rm rad}$, it is a good approximation as long as the parent distribution does not vary much on the spatial scale of $l_{\rm rad}$. Actually, even if the parent distribution varies linearly with radius, the approximation remains good. The probability $\mathrm{d}\mathcal{P}$ that a radioactive nucleus detected at the center of the hole has been created by a spallation at a distance between r and $r + \mathrm{d}r$ can be computed explicitly in the simple model described in Sect. 4.1, and it is found that (see Appendix for the demonstration)

$$\mathrm{d}\mathcal{P}(\text{emitted between } r \text{ and } r+\mathrm{d}r | \text{detected at center}) \propto \Theta(r - r_{\rm hole})\, N_{\rm parent}(r)\, \mathrm{e}^{-r/l_{\rm rad}}\, \mathrm{d}r \qquad (18)$$

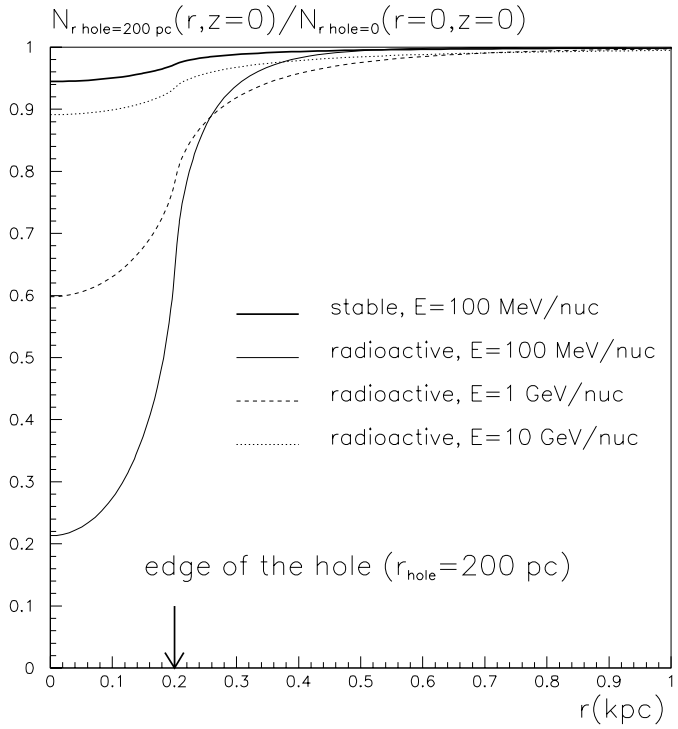

Fig. 5. Radial distribution of a radioactive species in the disc, across the hole, for $r_{\rm hole} = 200$ pc. Numerical values were taken for ^{26}Al (radioactive) and ^{28}Si (stable). The distribution of radioactive is very sensitive to the presence of the hole. However this effect is local and vanishes at several $r_{\rm hole}$. On the contrary, the distribution of stable species is not much affected.

so that most of the radioactive nuclei come from a ring extending from the edge of the hole ($r = r_{\rm hole}$) to a few $l_{\rm rad}$ away. As a result, if the parent nucleus density is not uniform, the spallation rate is determined by the effective density obtained as the average over the disc with the appropriate weight, given in the expression A.1 (see Appendix)

$$N_{\rm parent}^{\rm effective} = \frac{\iint {\rm d}^2\boldsymbol{r}\, N_{\rm parent}^2(\boldsymbol{r})\, \Theta(r - r_{\rm hole})\, \exp(-r/l_{\rm rad})}{\iint {\rm d}^2\boldsymbol{r}\, N_{\rm parent}(\boldsymbol{r})\, \Theta(r - r_{\rm hole})\, \exp(-r/l_{\rm rad})}.$$

We have compared this effective parent density to the actual parent density $N_{\rm parent}(R_\odot, z = 0)$ at the location of the Sun. For hole radii $r_{\rm hole} < 400$ pc and for $l_{\rm rad} < 5$ kpc, the difference is less than one percent at 10 GeV/nuc, and is completely negligible for $E \lesssim 1$ GeV/nuc.

4.5. Energy losses and reacceleration

In homogeneous models, the energy changes induced by energy losses and reacceleration are described by the equation (see Paper I and Paper II)

$$A_i N_i + 2h \frac{\partial}{\partial E} \left\{ b(E) N_i(E) - K_{EE} \frac{\partial N_i}{\partial E} \right\} = A_i N_i^{(0)} \tag{19}$$

where N_i is the Bessel transform of the final flux and $N_i^{(0)}$ is the initial flux (before energy losses and reacceleration are applied). Because of the hole, the energy loss term $b(E)$ now has a spatial dependence. It has the same value as above, except in the hole where there is no matter to interact with, so that

$b(r, E) = \Theta(r - r_{\rm hole}) b(E)$.

Thus, the Bessel transform of the quantity $\Theta(r - r_{\rm hole}) N(r, E)$, denoted $\mho_i$, must be introduced. As the spatial dependence of this function is exactly the same as the spallation term of the previous section, it is straightforward to write (see Eq. (12))

$$\begin{aligned} \mho_i(E) \;=\; & N_i(E) \left\{ 1 + \frac{r_{\rm hole}^2}{R^2 J_1^2(\zeta_i)} \left[J_0^2 \left(\frac{\zeta_i r_{\rm hole}}{R} \right) + J_1^2 \left(\frac{\zeta_i r_{\rm hole}}{R} \right) \right] \right\} \\ - \; & \frac{2 r_{\rm hole}}{R J_1^2(\zeta_i)} \sum_{j \neq i} \frac{N_j}{\zeta_j^2 - \zeta_i^2} \left[-\zeta_i J_0 \left(\frac{\zeta_j r_{\rm hole}}{R} \right) J_1 \left(\frac{\zeta_i r_{\rm hole}}{R} \right) + \zeta_j J_1 \left(\frac{\zeta_j r_{\rm hole}}{R} \right) J_0 \left(\frac{\zeta_i r_{\rm hole}}{R} \right) \right], \end{aligned} \tag{20}$$

so that $b(E)N_i(E)$ in (19) has to be replaced by $b(E)\mathcal{O}_i(E)$. It is again a coupled set of equations. The same perturbative approach as before is used: the new quantities $N_i^{(1)}$ affected by energy losses are estimated by replacing N_i by $N_i^{(0)}$. The new set $N_i^{(1)}$ is then inserted instead of $N_i^{(0)}$, etc. until convergence is reached. It is found that even in the presence of energy losses and reacceleration, the dependence on the hole radius is still very well described by (16).

We note that reacceleration has a negligible effect on radioactive propagation, which may be understood as it takes much longer than the lifetime $\gamma\tau_0$ to significantly reaccelerate a nucleus.

4.6. Conclusion and inclusion in the propagation code

The presence of a hole of radius $r_{\rm hole}$ lowers the radioactive flux by a factor given with a good precision by $\exp(-r_{\rm hole}/l_{\rm rad})$ where $l_{\rm rad}$ is given in (17).

It is not possible in practice to directly use the analytical formulæ described above because the double sums over Bessel indices are far too time consuming. Indeed, the accurate description of the hole requires a development of all functions over at least the $N \gg R/r_{\rm hole}\pi \sim 100$ first functions $J_0(\zeta_i x)$. We used $N = 5000$, for which a very good convergence of the Bessel series was achieved, and the double summation takes $N^2 = 2.5 \times 10^7$ elemental steps for each iteration and each model. The computation time required to apply these formulæ to all the models would have been too large.

Thus, we preferred to take advantage of the exponential dependence discussed above, and the flux of a given radioactive nucleus in the presence of a hole is obtained from each model with no hole by a multiplication by $\exp(-r_{\rm hole}/l_{\rm rad})$.

5. Experimental data and configurations of parameter space

We now turn to the more standard diffusion aspects of propagation. The main ingredients of our diffusion model have been widely depicted in Paper I, and we will not be exhaustive about them here. Instead, we simply motivate the choice of configurations that are used in this paper. We also review the experimental data that we compared to our calculations.

5.1. Sets of configurations used for the analysis

Propagation is assumed to be a diffusive process occurring both in the galactic disc and in a halo of thickness L. This process is characterized by an energy–dependent diffusion coefficient of the form $K(E) = K_0\beta\mathcal{R}^\delta$ where K_0 and δ are parameters of the model and $\mathcal{R}$ is the rigidity. Propagation is affected by a galactic wind $V_{\rm c}$ perpendicular to the galactic plane and by the presence of Alfvén waves of velocity $V_{\rm a}$. These are the five parameters of the model. All the sets of parameters consistent with measurements of stable nuclei analysis have been extracted and discussed in Paper I (see this paper for a detailed presentation of the model and more specifically Figs. 7 and 8). These sets of parameters are also consistent with the antiproton spectrum, as shown in Paper II.

Some further cuts in our initial sets of parameters could probably be applied on physical grounds (see for example the discussion on the Alfvénic velocity $V_{\rm a}$ in Sect. 5.2, Paper II). We adopted a conservative attitude and used the whole set, as the aim of this paper is precisely to explore whether it is possible to obtain further constraints on these parameters from the study of radioactive species.

5.2. The data set we used

Several experiments in the last twenty or thirty years have measured radioactive isotopes in cosmic rays with increasing precision, at energies of a few hundred MeV/nuc. The early data – usually presented as the ratio of the radioactive isotope to its stable companion(s) – were affected by errors of around 25–30%. The latest published data have error bars reduced by a factor of two or three. In the following, we implicitly refer to three satellite experiments, namely Voyager, Ulysses and ACE. Other experiments will sometimes be shown on figures but they will be purely illustrative since their accuracy is far smaller.

The best measured ratio is probably ^{10}Be/^{9}Be which corresponds to the lowest Z β–radioactive nucleus. Data from Ulysses (Connell 1998) and from ACE (Binns et al. 1999) are consistent, the quoted error bars being smaller for ACE. They are also consistent with the Voyager data point (Lukasiak et al. 1999) for which the quoted error is larger. We do not use the SMILI data, as the possibility that they are due to a statistical fluctuation is not ruled out (Ahlen et al. 2000).

As regards the radioactive chlorine isotope ^{36}Cl, results are usually provided as ^{36}Cl to total Cl ratio. The only available data, to our knowledge, are those from Ulysses (Connell et al. 1998) with a 1σ error of about 35%, and ACE (Binns et al. 1999) whose errors (even taken at 3σ) are completely included in the Ulysses 1-σ upper error band.

We finally end with the ^{26}Al/^{27}Al ratio. Contrary to other radioactive ratios, the measurements show more problems. Indeed, 1σ data from Ulysses (Simpson & Connell 1998) and ACE (Binns et al. 1999) exclude each other (the ACE central point is much lower than Ulysses'). Enlarging ACE error bars (which are smaller than Ulysses) to 3σ does not improve the compatibility. On the other hand, Ulysses data are fully compatible with 1σ Voyager data (Lukasiak et al. 1994), whose uncertainty is still much greater than for the other two experiments. The possible discrepancy between some of these data will be addressed later.

6. Results

We now present our analysis of the radioactive nuclei abundances. First, in the diffusion model with no hole (hereafter the *homogeneous model*), we can compute the expected flux of radioactive nuclei for each set of diffusion parameters given by the analysis of stable nuclei (Paper I) and compare to the data. Then, the presence of a local underdense region discussed above is tested, and the radius $r_{\rm hole}$ of this region is introduced as an additional parameter. The corresponding models will be called *inhomogeneous models*. As the stable nuclei are almost not affected by the presence of the hole (see Fig. 5), the sets of diffusion parameters given in Paper I are also used in the inhomogeneous case.

To sum up the procedure, the sets of diffusion parameters (K_0, L, δ, $V_{\rm a}$ and $V_{\rm c}$) given in Paper I are used to compute the radioactive nuclei fluxes, for different hole radii $r_{\rm hole}$. The special case $r_{\rm hole} = 0$ corresponds to the homogeneous models.

We proceed as follows. We first focus independently on the ^{10}Be/^{9}Be and ^{36}Cl/Cl ratios. They are computed for all the sets of diffusion parameters compatible with B/C (given in Paper I) and for several hole radii $r_{\rm hole}$. The constraints they induce on the parameters are studied. We then analyze simultaneously the two ratios ^{10}Be/^{9}Be and ^{36}Cl/Cl and finally the three ratios ^{10}Be/^{9}Be, ^{36}Cl/Cl and ^{26}Al/^{27}Al.

6.1. Constraints from ^{10}Be/^{9}Be

6.1.1. Comparison to ACE data

To begin with, we consider only the ^{10}Be/^{9}Be ratio, for which we have three compatible measurements. This is also the ratio for which an accurate spectrum is likely to be available in a near future (by ISOMAX, AMS, ...). This ratio is computed for each of the 5-parameter sets compatible with B/C given in Paper I, and for several hole radii $r_{\rm hole}$. The result is compared to the ACE data and the parameters giving a ratio falling out of the 3σ ACE error bars are discarded. We also do the same with a more stringent limit of 1σ, and the results are shown in the left panels of Fig. 6, where the scatter of the configurations is plotted in the plane δ–L for the homogeneous case, and δ–$r_{\rm hole}$ in the inhomogeneous one. For illustrative purpose, we also show on the right panels of Fig. 6 the result of the same procedure with 3σ and 1σ ^{36}Cl/Cl ACE data. The dots in this figure are merely the models obtained in the Paper I analysis.

The upper figure shows that for homogeneous models, the ^{10}Be/^{9}Be ratio alone further constrains L to a smaller region of the parameter space. For inhomogeneous models (lower part), the hole radius is constrained to values $r_{\rm hole} \lesssim 100$ pc. This can be easily understood: the value of ^{10}Be/^{9}Be in an inhomogeneous model is given by the corresponding value in a homogeneous model, decreased by the exponential factor $\exp(-r_{\rm hole}/l_{\rm rad})$. As the initial homogeneous parameter sets compatible with B/C give a wide range of ^{10}Be/^{9}Be values, those which are larger than the data are redeemed in inhomogeneous models. For holes larger than 100 pc, the exponential decrease is too important and theoretical predictions are too low to fit ACE data.

If we do not believe in the presence of the bubble, then our conclusions are similar to previous works: higher values of L are preferred in homogeneous models ($L \gtrsim 4$ kpc). For inhomogeneous models (including $r_{\rm hole} = 0$), the allowed ranges for the other diffusion parameters are not much affected if compared to the results of the stable nuclei analysis (Paper I). The ^{36}Cl/Cl ratio yields similar conclusions.

6.1.2. Discussion

Here we want to discuss qualitatively two other important points: the spectral behaviour and the interrelation of the three radioactive ratios. It will allow a more intuitive grasp of the combined analysis presented in the next section.

We first select all the homogeneous models compatible with ^{10}Be/^{9}Be (1σ and 3σ ACE data). Then, for each point of the resulting subset, the full propagation code is run and for the three radioactive species, maximal and minimal ratios are calculated at all energies and generate an envelope. These envelopes are represented in the upper part of Fig. 7. They contain all the allowed values of the above-mentioned ratios which are "compatible with B/C" and "compatible with ^{10}Be/^{9}Be ACE data 1σ". The same procedure is applied to the inhomogeneous models $r_{\rm hole} = 80$ pc (this value will be favored in the combined analysis).

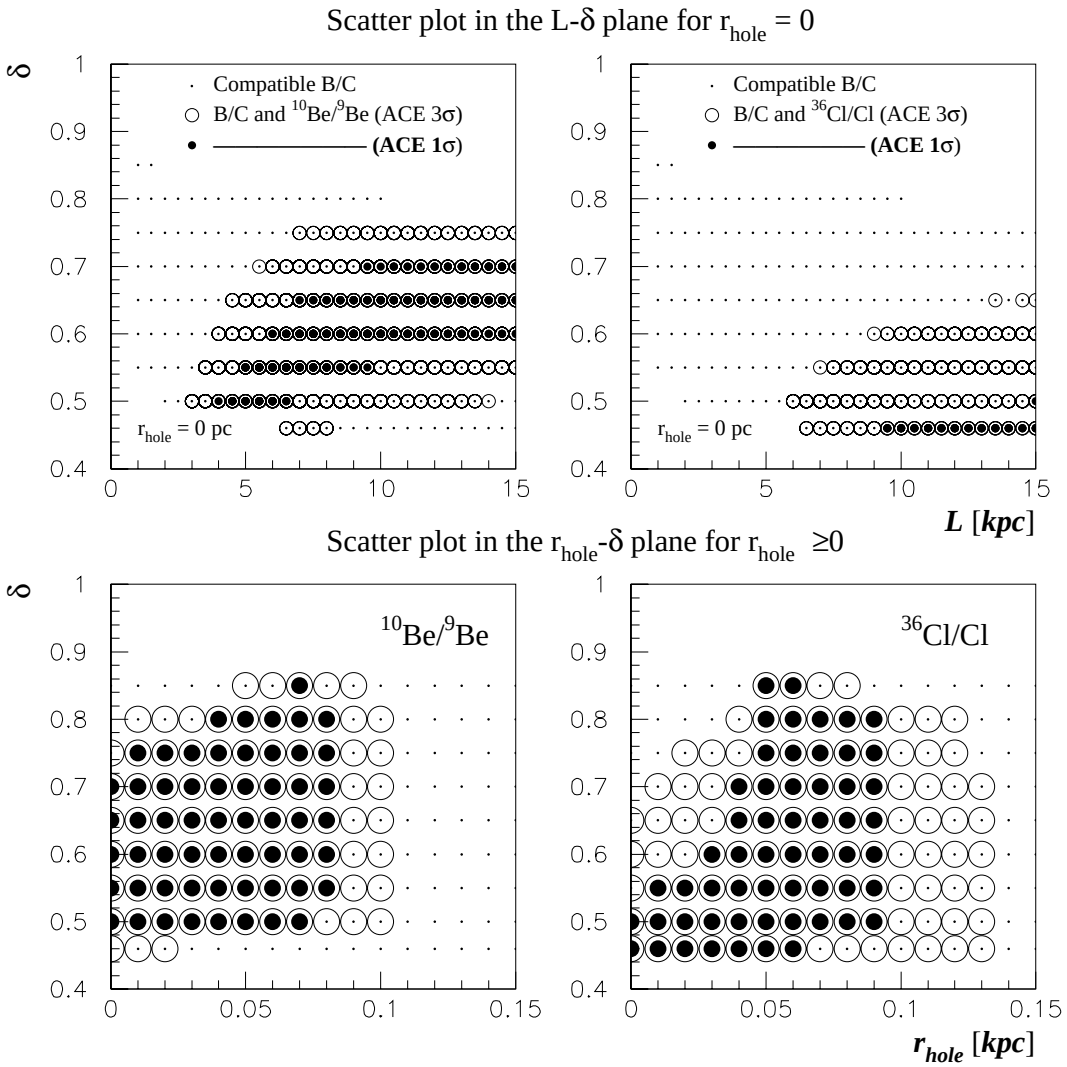

Fig. 6. Representation of the models compatible with combination of B/C (see Paper I) and various radioactive ACE data. See text and notations in the figure. Upper panels display homogeneous models ($r_{\rm hole} = 0$) in the plane L–δ. Lower panels display inhomogeneous models ($r_{\rm hole} \geq 0$) in the plane $r_{\rm hole}$–δ.

We now want to address the following questions: (i) is it possible, from the radioactive spectra, to experimentally distinguish inhomogeneous from homogeneous models, (ii) is it possible to break the degeneracy in the propagation parameters, and (iii) what would be a clear signature of the presence of the hole?

As regards the first question, the upper left panel (^{10}Be/^{9}Be) clearly shows that the answer is no, as even for extreme models ($r_{\rm hole} \sim 80$ pc), there is still an overlap between the homogeneous and inhomogeneous envelopes. Concerning question (ii), a partial answer has been given in the previous section: the ^{10}Be/^{9}Be ratio is degenerate in the diffusion parameters at the ACE energy. Figure 7 shows that it is actually true for all energies. We finally turn to question (iii). From left to right panels of Fig. 7, the nuclei have smaller and smaller lifetimes, so that the influence of the hole is larger and larger. In particular, the ratio ^{36}Cl/Cl is the most sensitive to $r_{\rm hole}$, and at low energy, homogeneous and inhomogeneous envelopes (for $r_{\rm hole} = 80$ pc) do not overlap. We thus expect that the combination of these ratio may break the degeneracy in $r_{\rm hole}$.

We also show, in the lower part of Fig. 7, the envelopes obtained as above but with the weaker constraint that ^{10}Be/^{9}Be is in the 3σ ACE error bars. For $r_{\rm hole} = 80$ pc and at the ACE data energy, the ^{10}Be/^{9}Be is never larger than 0.12, which corresponds to the largest ^{10}Be/^{9}Be obtained in the homogeneous models, decreased by the corresponding exponential factor. This is not shown in the figures, but for $r_{\rm hole} = 50$ pc, the lower panel dotted lines would be almost superimposed on the solid lines, whereas for $r_{\rm hole} = 100$ pc, they would only delimitate a very narrow strip. We also see that inhomogeneous models ($r_{\rm hole} = 80$ pc) are favored by the ^{36}Cl/Cl data. On the other hand, all the models compatible with ^{10}Be/^{9}Be clearly fail to reproduce the 3σ ACE ^{26}Al/^{27}Al data.

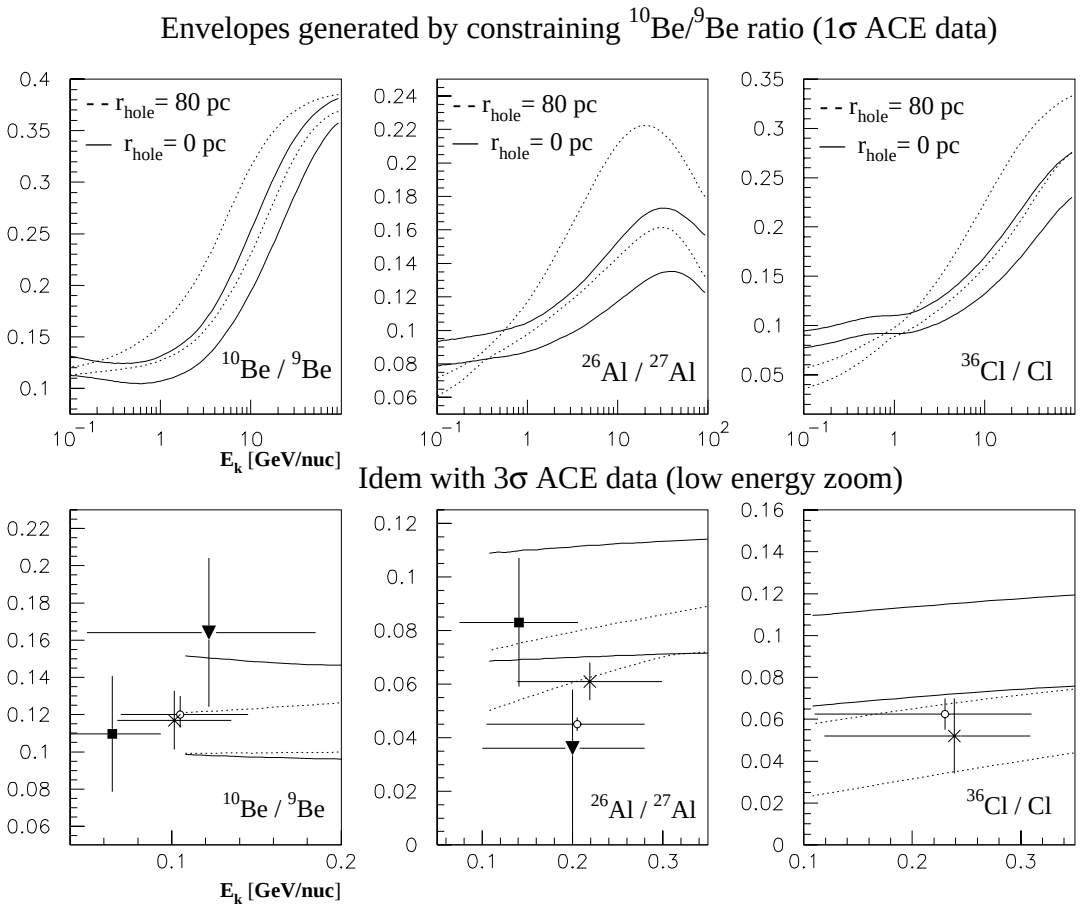

Fig. 7. Envelopes of the spectra obtained with all the models compatible with ^{10}Be/^{9}Be ACE 1σ (upper) and 3σ (lower) for the three radioactive species. Solid lines are for homogeneous models ($r_{\rm hole} = 0$ pc) and dashed lines are for inhomogeneous models ($r_{\rm hole} = 80$ pc). Data in the lower panel are from ACE (circles), Ulysses (crosses), Voyager (filled squares) and ISEE (filled triangles, Wiedenbeck 1985).

6.2. Combined analysis of ^{10}Be/^{9}Be and ^{36}Cl/Cl

We now analyze simultaneously the two ratios ^{10}Be/^{9}Be and ^{36}Cl/Cl. From the initial set of parameters compatible with B/C, we select those giving values of ^{10}Be/^{9}Be and ^{36}Cl/Cl in the error bars of ACE (1σ and 3σ). As expected from Fig. 6, there is no homogeneous model which fulfills the above condition at 1σ (the two regions delimited by the filled circles in the left and right panels do not overlap). This can be seen in Fig. 8 which displays the models compatible with ACE at the 1σ (filled circles) and 3σ (empty circles) level. We saw in the previous section that high values of L are independently favored by the two ratios ^{10}Be/^{9}Be and ^{36}Cl/Cl for homogeneous models, and it is natural to recover this trend in the combined analysis, which points towards $L \gtrsim 6$ kpc at the 3σ level. The allowed range for the other parameters are not much changed.

As regards the influence of $r_{\rm hole}$, we see that the combined analysis naturally favors hole radii 60 pc $\lesssim r_{\rm hole} \lesssim$ 80 pc (as seen before, values $r_{\rm hole} \gtrsim 100$ pc are independently excluded at the 3σ level), which is in full agreement with LISM observations. Note that for these particular models, values $L \gtrsim 12$ kpc are excluded at the 1σ level.

6.3. Combined analysis all three radioactive: Problem with data?

The next logical step is to include the ^{26}Al/^{27}Al ratio in the analysis. We first display in Fig. 9 the values of this ratio for the models discussed in the previous section, i.e. compatible with ^{10}Be/^{9}Be and ^{36}Cl/Cl ACE data at 3σ. We also show the ^{26}Al/^{27}Al experimental bounds from ACE and Ulysses at 3σ.

The first strong conclusion is that all these models (homogeneous and inhomogeneous) give similar ^{26}Al/^{27}Al values at $\sim$200 MeV/nuc. Moreover, it is seen that these values are not compatible with ACE data, even at the 6σ level. We will come back to this point later on. As pointed out in Sect. 5.2, other experiments are not compatible with the ACE data for this particular ratio. To consider the possibility that the ^{26}Al/^{27}Al value may be higher than hinted by the ACE measurement; we repeat the previous analysis applying Ulysses data for this ratio.

In Fig. 10, we show the models compatible with the ^{10}Be/^{9}Be and ^{36}Cl/Cl ACE 3σ data, plus the ^{26}Al/^{27}Al Ulysses 3σ data (open circles) and 1σ data (filled circles). In the latter case, only inhomogeneous models with $r_{\rm hole} \approx 100$ pc are consistent with the experimental values for the three ratios. In particular, we emphasize that homogeneous models are excluded.

However, it must be stressed that for these "good" models, the ^{10}Be/^{9}Be and ^{36}Cl/Cl ratios have the lowest possible value still compatible with 3σ ACE data, whereas the ^{26}Al/^{27}Al ratio has the maximal value compatible with 1σ Ulysses data, so that these ratio are only marginally consistent. In Fig. 11, we also present the envelopes obtained as in the previous section, but with the more stringent condition that the ^{10}Be/^{9}Be and ^{36}Cl/Cl ratios are within the 1 σ ACE error bars.

We did not make the analysis with the Voyager data point instead of Ulysses because the error bars are much larger. However, we notice that the central value provided by this experiment is in better agreement with our derived ^{26}Al/^{27}Al ratios (see Fig. 7).

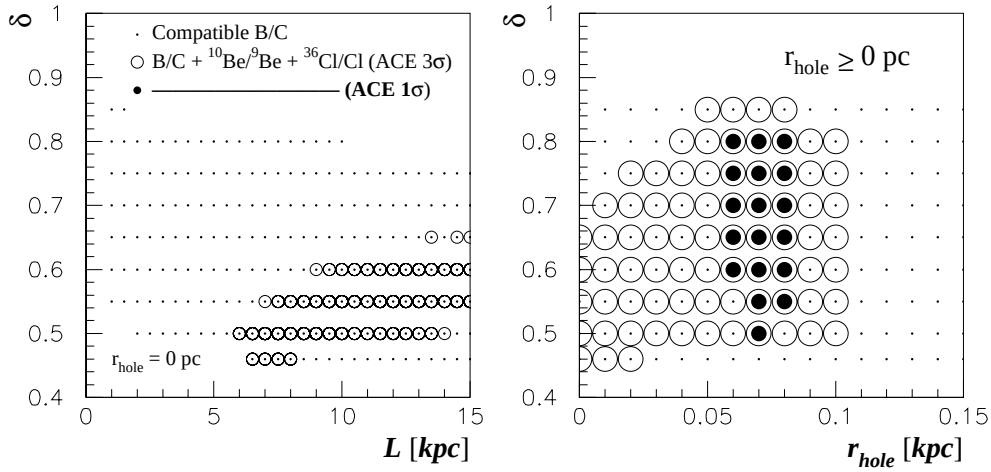

Fig. 8. Representation of the models compatible with B/C plus both ^{10}Be/^{9}Be and ^{36}Cl/Cl ACE 3σ (open circles) and 1σ (filled circles). Left panel displays homogeneous models ($r_{\rm hole} = 0$) in the plane L–δ. Right panel displays inhomogeneous models ($r_{\rm hole} \geq 0$) in the plane $r_{\rm hole}$–δ.

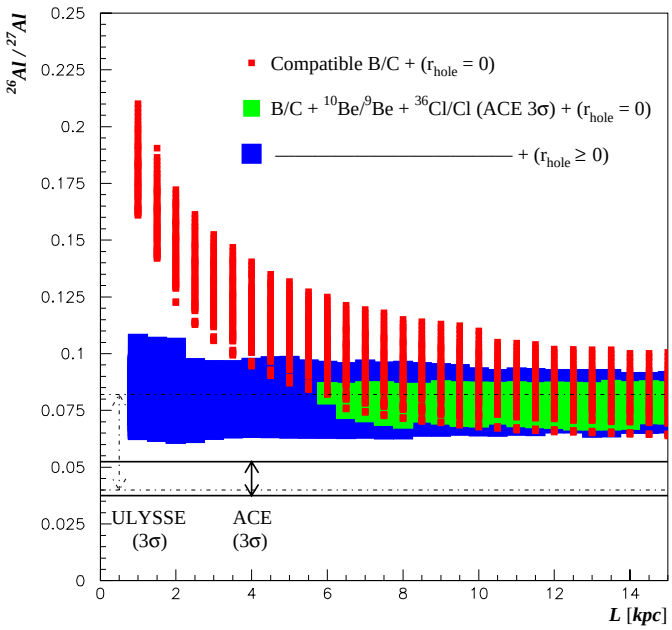

Fig. 9. Representation of the ^{26}Al/^{27}Al ratio at the ACE energy as a function of L for the models compatible with (i) B/C in homogeneous models (small squares), (ii) B/C plus ^{10}Be/^{9}Be and ^{36}Cl/Cl ACE 3σ (medium squares are for homogeneous models and big squares are for inhomogeneous models). Solid lines represent the 3σ error band from ACE, dashed lines represent the 3σ error band from Ulysses.

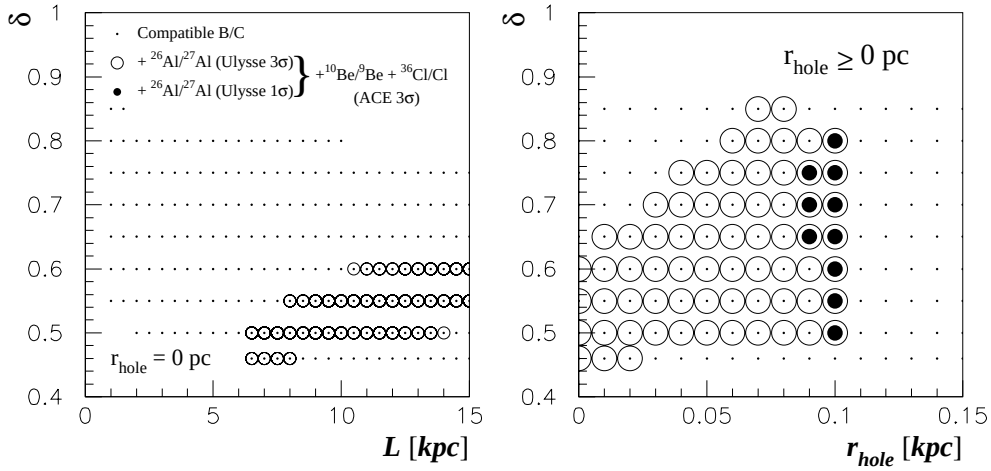

Fig. 10. Representation of the models compatible with B/C plus ^{10}Be/^{9}Be and ^{36}Cl/Cl ACE 3σ plus ^{26}Al/^{27}Al Ulysses 3σ (open circles) and 1σ (filled circles) data. Left panel displays homogeneous models ($r_{\rm hole} = 0$) in the plane L–δ. Right panel displays inhomogeneous models ($r_{\rm hole} \geq 0$) in the plane $r_{\rm hole}$–δ.

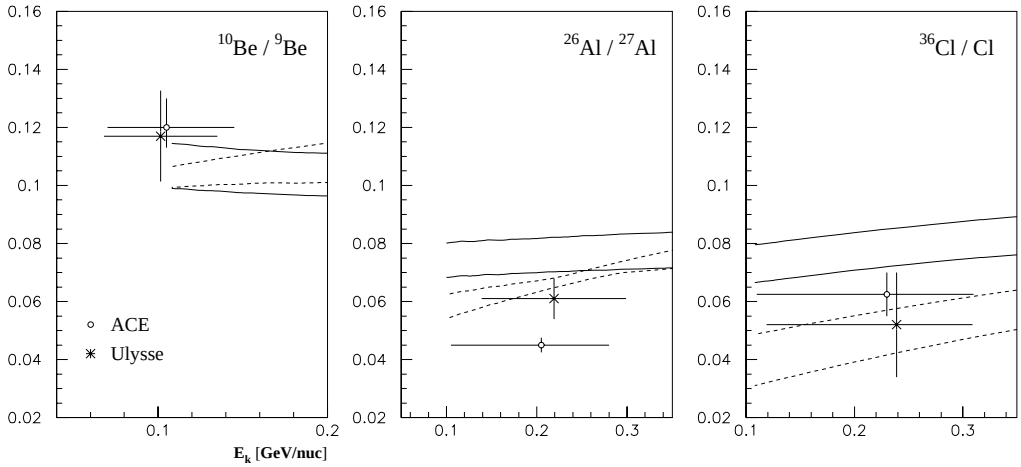

Fig. 11. Envelopes of the spectra obtained with all the models compatible with ^{10}Be/^{9}Be ACE and ^{36}Cl/Cl ACE 3σ plus ^{26}Al/^{27}Al Ulysses 3σ for the three radioactive species. Solid lines are for homogeneous models ($r_{\rm hole} = 0$) and dashed lines are for inhomogeneous models ($r_{\rm hole} \geq 0$). Data in the lower panel are from ACE (circles), Ulysses (crosses).

7. Conclusion and discussion

We have presented the analysis of the three radioactive ratios ^{10}Be/^{9}Be, ^{36}Cl/Cl and ^{26}Al/^{27}Al in the framework of a diffusion model, taking into account the presence of a local underdensity of radius $r_{\rm hole}$. We find that the ^{10}Be/^{9}Be and ^{36}Cl/Cl ratios are compatible with ACE data if $r_{\rm hole} \sim 60{-}80$ pc, but that no model is simultaneously compatible with the ACE data for the three ratios. However, if we consider other ^{26}Al/^{27}Al data (Ulysses or Voyager), some models are marginally consistent and the cases 60 pc $\lesssim r_{\rm hole} \lesssim$ 100 pc are preferred. These values are in agreement with independent estimations of LISM studies. The presence of this hole would also lead to an attenuation of the expected ^{14}C flux of the order of 10^{-4}. Thus, it seems a very difficult task to detect any ^{14}C in cosmic radiation, unless some local source is present. For example, radioactive nuclei could be produced in the very local fluff (with a very low density, see Sect. 3.2.1). This has been more realistically modelled by Ptuskin & Soutoul (1990) and Ptuskin et al. (1997) with a three-layer bubble. It would be straightforward to adapt our model to take into account a multi-shell contribution (as long as the symmetry is preserved). Moreover, all these models assume that the shells have the same center, which is surely wrong, but the generic behaviour in $\exp(-r_{\rm hole}/l_{\rm rad})$ is expected to hold even in a more complicated geometry.

We have not yet discussed solar modulation. All the data have slightly different solar modulation parameters. We used the simple force field scheme to modulate our fluxes (as in Papers I and II). We checked that even taking extreme values for the modulation parameters yields about 5% changes in calculated ratio. This does not affect the results of our analysis.

Our results point out an important feature of cosmic rays. Either there is a problem with the Al data, or there is a fundamental problem with the diffusive approach of radioactive nuclei propagation. Alternatively, there could be a problem with cross sections. Other similar studies (see for example Strong & Moskalenko 1998 and further developments) should be able to confirm our results when incorporating a hole in their model.

Acknowledgements. F.D. gratefully acknowledges a fellowship by the Istituto Nazionale di Fisica Nucleare. We also would like to thank the French Programme National de Cosmologie for its financial support.

Appendix A: Demonstration of formula (18)

In this section, we compute the probability $\mathrm{d}\mathcal{P}$ that a radioactive nucleus detected at the center of the hole has been created by a spallation at a distance between r and $r+\mathrm{d}r$, in the framework of the simple modelling of Sect. 4.1. It is a conditional probability, and as such it can be expressed, using Bayes theorem, by

$$\begin{aligned}\mathrm{d}\mathcal{P}\left\{\text{created at } r|\text{detected in 0}\right\} &= \mathcal{P}\left\{\text{detected in 0}|\text{created at } r\right\} \times \frac{\mathrm{d}\mathcal{P}\left\{\text{created at } r\right\}}{\mathcal{P}\left\{\text{detected in 0}\right\}} \\ &\propto \mathcal{P}\left\{\text{detected in 0}|\text{created at } r\right\} \times \mathrm{d}\mathcal{P}\left\{\text{created at } r\right\}.\end{aligned}$$

The first term is given by the expression (4)

$$\mathcal{P}\left\{\text{detected in 0}|\text{created at } r\right\} \propto \int_0^\infty \exp\left\{-\frac{r^2}{4Kt}-\frac{t}{\gamma\tau_0}\right\}\frac{\mathrm{d}t}{t^{3/2}}$$

and the second term is simply given by

$$\mathrm{d}\mathcal{P}\left\{\text{created at } r\right\} = \frac{\Theta(r-r_{\rm hole})\,2\pi r\,N(r)\,\mathrm{d}r}{\int 2\pi r N(r)\,\mathrm{d}r} \propto \Theta(r-r_{\rm hole}) r N(r)\,\mathrm{d}r$$

where $N(r)$ is the density of parent nuclei. This gives

$$\mathrm{d}\mathcal{P}\left\{\text{created at } r|\text{detected in 0}\right\} \propto \Theta(r-r_{\rm hole})\,r\,N(r)\,\mathrm{d}r \times \int_0^\infty \exp\left\{-\frac{r^2}{4Kt}-\frac{t}{\gamma\tau_0}\right\}\frac{\mathrm{d}t}{t^{3/2}}.$$

Defining $x = r/\sqrt{4Kt}$, the integral is proportional to

$$\int_0^\infty \exp\left\{-\frac{r^2}{4K\gamma\tau_0 x^2}-x^2\right\}\mathrm{d}x.$$

The value of this integral is given by (5) which gives

$$\mathrm{d}\mathcal{P}\left\{\text{created at } r|\text{detected in 0}\right\} \propto \Theta(r-r_{\rm hole})\,N(r)\,\mathrm{e}^{-r/l_{\rm rad}}\mathrm{d}r. \tag{A.1}$$

The proportionality coefficient of this relation would easily be obtained by imposing that $\int_{r=0}^{\infty}\mathrm{d}\mathcal{P}=1$.

References

Adams, J. H., Silberberg, R., & Tsao, C. H. 1985, ApJS, 114, 365
Ahlen, S. P., Greene, N. R., Loomba, D., et al. 2000, ApJ, 534, 757
Audi, G., Bersillon, O., Blachot, J., & Wapstra, A. H. 1997, Nucl. Phys. A, 624, 1
Binns, W. R., et al. 1999, ICRC 26 Salt Lake City, OG-1.1.06
Breitschwerdt, D., Freyberg, M. J., & Egger, R. 2000, A&A, 361, 303
Cassé, M. 1973, ApJ, 180, 623
Connell, J. J. 1998, ApJ, 501, L59
Connell, J. J., DuVernois, M. A., & Simpson, J. A. 1998, ApJ, 501, L97
Cox, D. P. 1997, IAU Colloq. 166, Germany, ed. D. Breitschwerdt, M. J. Freyberg, & J. Truemper, 121
Cox, D. P., & Reynolds, R. J. 1987, ARA&A, 25, 303
Donato, F., Maurin, D., Salati, P., et al. 2002, ApJ, 563, 1
Freier, P. S., Young, J. S., & Waddington, C. J. 1980, ApJ, 240, L53
Fruscione, A., Hawkins, I., Jelinsky, P., & Wiercigrosh, A. 1994, ApJS, 94, 127
Garcia-Munoz, M., Mason, G. M., & Simpson, J. A. 1977, ApJ, 217, 859
Ginzburg, V. L., Khazan, Ya. M., & Ptuskin, V. S. 1980, Ap&SS, 68, 295
Goldman, D. T. 1982, American Institute of Physics Handbook, third edition
Hagen, F. A., Fisher, A. J., & Ormes, J. F. 1977, ApJ, 212, 262

Leske, R. A. 1993, ApJ, 405, 567
Letaw, J. R., Silberberg, R., & Tsao, C. H. 1984, ApJS, 56, 369
Linsky, J. L., Redfield, S., Wood, B. E., & Piskunov, N. 2000, ApJ, 528, 756
Lukasiak, A., McDonald, F. B., & Webber, W. R. 1994, ApJ, 430, L69
Lukasiak, A., McDonald, F. B., & Webber, W. R. 1999, ICRC 26 Salt Lake City, OG-1.1.12
Lund Fisker, J., Martínez-Pinedo, G., & Langanke, K. 1999, EPJA, 5, 269
Martínez-Pinedo, G., & Vogel, P. 1998, Phys. Rev. Lett., 81, 281
Maurin, D., Donato, F., Taillet, R., & Salati, P. 2001, ApJ, 555, 585 (Paper I)
McKee, C. F. 1998, IAU Colloq. 166, Germany, ed. D. Breitschwerdt, M. J. Freyberg, & J. Truemper, 565
Morfill, G. E., & Freyberg, M. J., IAU Colloq. 166, Germany, ed. D. Breitschwerdt, M. J. Freyberg, & J. Truemper, 177
Osborne, J. L., & Ptuskin, V. S. 1987, Sov. Astron. Lett., 13, 980
Prishchep, V. L., & Ptuskin, V. S. 1975, Ap&SS, 32, 265
Ptuskin, V. S., & Soutoul, A. 1990, A&A, 237, 445
Ptuskin, V. S., & Soutoul, A. 1998, A&A, 337, 859
Ptuskin, V. S., Jones, F. C., Ormes, J. F., & Soutoul, A. 1997, Adv. Space Res., 19, 787
Reames, D. V. 1970, ApJ, 162, 837
Sfeir, D. M., Lallement, R., Crifo, F., & Welsh, B. Y. 1999, A&A, 346, 785
Simpson, J. A., & Connell, J. J. 1998, ApJ, 497, L88
Simpson, J. A., & Garcia-Munoz, M. 1987, Space Sci. Rev., 46, 205
Smith, R. K., & Cox, D. P. 2001, ApJS, 134, 283
Strong, A. W., & Moskalenko, I. V. 1998, ApJ, 509, 212
Tripathi, R. K., Cucinotta, F. A., & Wilson, J. W. 1997a, NASA Technical Paper, 3621
Tripathi, R. K., Cucinotta, F. A., & Wilson, J. W. 1997b, NASA Technical Paper, 3656
Tripathi, R. K., Cucinotta, F. A., & Wilson, J. W. 1999, NASA Technical Paper, 209726
Webber, W. R., Lezniak, J. A., Kish, J. C., & Simpson, G. A. 1977, Astrophys. Lett., 18, 125
Webber, W. R., Kish, J. C., & Schrier, D. A. 1990, Phys. Rev. C, 41, 566
Webber, W. R., Lee, M. A., & Gupta, M. 1992, ApJ, 390, 96
Webber, W. R., Soutoul, A., Kish, J. C., et al. 1998, Phys. Rev. C, 58 3539
Welsh, B. Y., Craig, N., Vedder, P. W., & Vallerga, J. V. 1994, ApJ, 437, 638
Wiedenbeck, M. E. 1985, ICRC, 19 2, 84